Inorg. Chem. **2004**, *43*, 7741–7751

Synthesis and Characterization of Nitrosyl Diruthenium Complexes. Interaction between NO and CO across the Metal–Metal Bond

Baocheng Han,*,†,‡ Jianguo Shao,‡ Zhongping Ou,‡ Tuan D. Phan,‡ Jing Shen,‡ John L. Bear,*,‡ and Karl M. Kadish*,‡

Departments of Chemistry, University of Wisconsin—Whitewater, Whitewater, Wisconsin 53190, and University of Houston, Houston, Texas 77204-5003

Received July 27, 2004

Two neutral diruthenium complexes and one anionic diruthenium complex, $Ru_2(dpf)_4(NO)$, $Ru_2(dpf)_4(NO)_2$, and $[Ru_2(dpf)_4(NO)]^-$, where dpf is diphenylformamidinate anion, were synthesized and characterized as to their electrochemical and spectroscopic properties. Two of the compounds, $Ru_2(dpf)_4(NO)$ and $Ru_2(dpf)_4(NO)_2$, were also structurally characterized. $Ru_2(dpf)_4(NO)$ undergoes reversible one-electron reductions under N_2 at $E_{1/2}$ = 0.06 and –1.24 V in CH_2Cl_2, 0.1 M TBABr. These processes are shifted to $E_{1/2}$ = 0.18 and –0.78 V under CO due to the trans-coordination of a CO molecule which stabilizes the singly and doubly reduced forms of the metal–metal bonded complexes, thus leading to easier reductions. CO does not coordinate to $Ru_2(dpf)_4(NO)$, but it does bind to the singly reduced species to generate $[Ru_2(dpf)_4(NO)(CO)]^-$ under a CO atmosphere in solution; characteristic NO and CO bands are seen for this compound at ν_{NO} = 1674 cm^{-1} and ν_{CO} = 1954 cm^{-1}. $Ru_2(dpf)_4(NO)_2$ displays a reversible one-electron reduction at $E_{1/2}$ = –1.24 V versus SCE and an irreversible reduction at E_{pc} = –1.96 V in CH_2Cl_2, 0.1 M TBAP under N_2. There are also two reversible one-electron oxidations at $E_{1/2}$ = 0.24 and 1.15 V. Spectroelectrochemical monitoring of the $Ru_2(dpf)_4(NO)_2$ oxidation processes in a thin-layer cell shows only a single NO vibration for each electrogenerated product and ν_{NO} is located at 1726 (neutral), 1788 (singly oxidized), or 1834 (doubly oxidized) cm^{-1}. Finally, a labile CO complex, $[Ru_2(dpf)_4(NO)(CO)]^-$, could be generated by passing CO into a solution of $[Ru_2(dpf)_4(NO)]^-$. Formation of the mixed CO/NO adduct was confirmed by electrochemistry and infrared spectroscopy. Analysis of the NO and CO stretching vibration frequencies for $[Ru_2(dpf)_4(NO)(CO)]^-$ by in-situ FTIR spectroelectrochemistry and comparisons with data for $Ru_2(dpf)_4(NO)$ and $Ru_2(dpf)_4(CO)$ reveal the presence of a strong interaction between NO and CO across the Ru–Ru bond.

Introduction

The chemistry of nitric oxide (NO) and carbon monoxide (CO) has been a traditionally interesting area for many decades since it is known that the binding of NO or CO to a metal center imparts a unique chemistry both to the metal center and the nitrosyl or carbonyl ligand itself.[1–3] Studies of NO received renewed interest in the early 1990s due to the discovery of its important roles in a large variety of biological functions and the use of metal nitrosyl complexes as agents potentially capable of releasing or removing NO.[4]

The synthesis and characterization of numerous diruthenium complexes with carboxylate type structures and various axial ligands have been reported in the literature since the 1960s.[5–16] The axial ligands in these compounds show a

* To whom correspondence should be addressed. E-mail: kkadish@uh.edu (K.M.K.).
† University of Wisconsin—Whitewater.
‡ University of Houston.

(1) *Advanced Inorganic Chemistry*, 6th ed.; Cotton, F. A., Wilkinson, G., Murillo, C. A., Bochmann, M., Eds.; John Wiley & Sons: New York, 1999.
(2) Richter-Addo, G. B. *Metal Nitrosyls*; Oxford University Press: Oxford, 1992.
(3) Nakamoto, K. *Infrared and Raman Spectra of Inorganic and Coordination Compounds*; Wiley-Interscience: New York, 1997.
(4) (a) Solomon, H. S. *Science* **1992**, *257*, 494. (b) Zhang, J.; Dawson, V. L.; Dawson, T. M.; Snyder, S. H. *Science* **1994**, *263*, 687. (c) Legzdins, P.; Retting, S. J.; Sayers, S. F. *J. Am. Chem. Soc.* **1994**, *116*, 105. (d) Davies, N. A.; Wilson, M. T.; Slade, E.; Fricker, S. P.; Murrer, B. A.; Powell, N. A.; Henderson, G. R. *Chem. Commun.* **1997**, 47. (e) Chanda, N.; Mobin, S. M.; Puranik, V. G.; Datta, A.; Niemeyer, M.; Lahiri, G. K. *Inorg. Chem.* **2004**, *43*, 1056. (f) McCleverty, J. A. *Chem. Rev.* **2004**, *104*, 403.
(5) Cotton, F. A.; Walton, R. A. *Multiple Bonds Between Metal Atoms*; Oxford University Press: Oxford, 1993.
(6) Lindsay, A. J.; Wilkinson, G.; Motevalli, M.; Hursthouse, M. B. *J. Chem. Soc., Dalton Trans.* **1987**, 2723.

10.1021/ic048983e CCC: $27.50
Published on Web 10/29/2004

range of σ basicities and π acidities. However, reports on diruthenium complexes with strong π acid NO or CO as an axial ligand are still rather rare in the literature.[6−9,12]

There are only three examples of diruthenium metal−metal bonded complexes with NO axial ligands which have been structurally characterized to date.[6,8] These are $Ru_2(C_2H_5CO_2)_4(NO)_2$,[6] $Ru_2(CF_3CO_2)_4(NO)_2$.[6] and $Ru_2(Fap)_4(NO)Cl$,[8] where Fap is the 2-fluoroanilinopyridinate anion. The first two compounds were formally described[6] as $Ru_2^{I,I}(NO^+)_2$ with the electronic configuration of $(\sigma)^2(\pi)^4(\delta)^2(\pi^*)^4(\delta^*)^2$ while the latter complex was assigned[8] as $Ru_2^{II,II}(NO^+)Cl$ with an electronic configuration of $(\sigma)^2(\pi)^4(\delta)^2(\pi^*)^3(\delta^*)^1$.

We earlier reported the synthesis and characterization of a stable diruthenium complex with CO as the axial ligand, $Ru_2(dpf)_4(CO)$.[7] The reduction by one-electron under N_2 leads to $[Ru_2(dpf)_4(CO)]^-$, but a second CO ligand is added under a CO atmosphere to yield $[Ru_2(dpf)_4(CO)_2]^-$ as the electroreduced product.[7] The electrogeneration of diruthenium complexes in low oxidation states under a CO atmosphere is well-documented,[7,9] and this fact is further explored in the present paper for the case of dpf complexes which are also axially coordinated with NO.

To our knowledge, there have been no reports in the literature describing diruthenium metal−metal bonded complexes with both NO and CO as axial ligands. It was thus our goal to synthesize and isolate a diruthenium complex with a single NO axial ligand so that it could provide us an opportunity to examine its chemical and electrochemical properties under CO to see if CO could bind to the second Ru atom upon reduction or oxidation or in its neutral state.

We now report the synthesis of one such compound, $Ru_2(dpf)_4(NO)$, which was characterized with respect to its structural, magnetic, electrochemical and spectroscopic properties under both N_2 and CO atmospheres. $Ru_2(dpf)_4(NO)_2$, $[Ru_2(dpf)_4(NO)]^-$ and $[Ru_2(dpf)_4(NO)(CO)]^-$ were also synthesized and examined as to their electrochemical, spectroscopic and/or structural properties and the data are then compared to $Ru_2(dpf)_4(NO)$ and $Ru_2(dpf)_4(CO)$ under the same experimental conditions.

Experimental Section

Chemicals. $Ru_2(CH_3CO_2)_4Cl$ and $Ru_2(dpf)_4Cl$ were prepared according to a method previously published in the literature.[15] Tetra-*n*-butylammonium perchlorate (TBAP) was purchased from Fluka Chemika Co., recrystallized from ethyl alcohol, and dried under vacuum at 40 °C for at least one week prior to use. Other supporting electrolytes were used as received. Ultrahigh-purity nitrogen, argon, carbon monoxide, and nitric oxide were purchased from Matheson Trigas Co. Carbon monoxide was passed through a CH_2Cl_2 bubbler, and nitric oxide was first passed through a sodium hydroxide pellet column, followed by bubbling through a water trap and then a CH_2Cl_2 trap prior to use. Absolute dichloromethane (CH_2Cl_2) was obtained from Fluka Chemical Co. and used as received. HPLC grade acetone, benzene, and hexanes (Aldrich Chemical Co.) were used directly.

Instrumentation and Physical Measurements. Cyclic voltammetry was carried out with an EG&G model 173 potentiostat. A three-electrode system was used and consisted of a glassy carbon or platinum disk working electrode, a platinum wire counter electrode, and a homemade saturated calomel electrode (SCE) as the reference electrode. The SCE was separated from the bulk of the solution by a fritted-glass bridge of low porosity which contained the solvent/supporting electrolyte mixture. All potentials are referenced to the SCE, and all measurements were carried out at room temperature.

Controlled-potential electrolysis was also carried out with an EG&G model 173 potentiostat. An "H" type cell was used for performing bulk electrolysis and consisted of two cylindrically shaped platinum gauze electrodes which served as a working and counter electrode and were separated from each other by a fine fitted disk. Elemental analysis was carried out by Quantitative Technologies Inc., Whitehouse, NJ.

UV−vis spectroelectrochemistry experiments were carried out with a Hewlett-Packard model 8453 diode array spectrophotometer. Infrared spectroelectrochemical measurements were made with a FT-IR Nicolet Magna-IR 550 spectrometer using a specially constructed light-transparent three-electrode cell. The IR spectra of each electro-oxidized or electroreduced complex under N_2 or CO were obtained as difference spectra measured against the corresponding neutral compound as background in CH_2Cl_2, 0.2 M TBAP or TBABr, after bubbling N_2 or CO through the spectroelectrochemical cell for 10 min prior to applying a potential. A blanket of N_2 or CO was maintained above the solution during the measurement.

^{1}H NMR measurements were recorded at room temperature on a General Electric QE-300 Plus spectrometer and were referenced to tetramethylsilane (TMS). ESR spectra were recorded on a Bruker ER 100E spectrometer. The g values were measured with respect to diphenylpicrylhydrazyl (DPPH: $g = 2.0036 \pm 0.0003$). Magnetic susceptibilities were measured according to the Evans method[17] on a General Electric QE-300 FT NMR spectrometer in CD_2Cl_2 with TMS as the internal reference compound. Mass spectra were recorded on an Applied Biosystem Voyager DE-STR MALDI-TOF mass spectrometer equipped with a nitrogen laser (337 nm) at the University of Houston Mass Spectrometry Laboratory.

Synthesis of $Ru_2(dpf)_4(NO)$. $Ru_2(dpf)_4(NO)$ was obtained by bubbling NO into the deaerated CH_2Cl_2 solution of $Ru_2(dpf)_4Cl$ at ambient temperature for 30 min. The color changed from yellow-green to brown during this period of time. After that, the solution was then purged with nitrogen for 1 h during which the color converted slowly from brown to green. The solution was finally exposed to air and was left overnight. Hexanes or acetones were added to precipitate $Ru_2(dpf)_4(NO)$, and the green-blue color precipitate was then collected and twice recrystallized with a yield of 90%. Crystals suitable for X-ray diffraction analysis were

(7) Kadish, K. M.; Han, B.; Shao, J.; Ou, Z.; Bear, J. L. *Inorg. Chem.* **2001**, *40*, 6848.
(8) Bear, J. L.; Wellhoff, J.; Royal, G.; Van Caemelbecke, E.; Eapen, S.; Kadish, K. M. *Inorg. Chem.* **2001**, *40*, 2282.
(9) Kadish, K. M.; Phan, T.; Giribabu, L.; Shao, J.; Wang, L.-L.; Thuriere, A.; Van Caemelbecke, E.; Bear, J. L. *Inorg. Chem.* **2004**, *43*, 1012.
(10) Bear, J. L.; Chen, W.-Z.; Han, B.; Huang, S.; Wang, L.-L.; Thuriere, A.; Van Caemelbecke, E.; Kadish, K. M.; Ren, T. *Inorg. Chem.* **2003**, *42*, 6230.
(11) Xu, G.-L.; Jablonski, C. G.; Ren, T. *J. Organomet. Chem.* **2003**, *683*, 388.
(12) Clark, D. L.; Green, J. C.; Redfern, C. M. *J. Chem. Soc., Dalton Trans.* **1989**, 1037.
(13) Wesemann, J. L.; Chisholm, M. H. *Inorg. Chem.* **1997**, *36*, 3258.
(14) Cotton, F. A.; Yokochi, A. *Inorg. Chem.* **1997**, *36*, 3258.
(15) Bear, J. L.; Han, B.; Huang, S.; Kadish, K. M. *Inorg. Chem.* **1996**, *35*, 3012.
(16) Kadish, K. M.; Wang, L.-L.; Thuriere, A.; Van Caemelbecke, E.; Bear, J. L. *Inorg. Chem.* **2003**, *42*, 834.
(17) Evans, D. F. *J. Chem. Soc.* **1959**, 2003.

obtained by a slow diffusion of hexanes or acetone into the CH_2Cl_2/benzene (98:2) solution of $Ru_2(dpf)_4(NO)$. Mass spectral data [*m*/*e*, (fragment)]: 983 $[Ru_2(dpf)_4]^+$. UV−vis spectrum in PhCN [λ, nm]: 455 and 690. Infrared spectrum (solid): 1773 (s), 1593 (m), 1557 (s), 1487 (s), 1384 (s), 1213 (s), 1092 (m) cm^{-1} (s, strong; m, medium). Anal. Calcd for $C_{52}H_{44}N_9ORu_2 \cdot CH_2Cl_2$: C, 57.98; H, 4.22; N, 11.48. Found: C, 55.29; H, 3.61; N, 11.08. Magnetic susceptibility (CD_2Cl_2 solution, 292 K): 4.01 μ_B.

Synthesis of $Ru_2(dpf)_4(NO)_2$. This compound was synthesized by passing NO for 30 min through a CH_2Cl_2, 0.2 M TBAP, solution of $Ru_2(dpf)_4$ which had been generated by bulk electrolysis of $Ru_2(dpf)_4Cl$ at −1.00 V versus SCE under Ar. During this process, the color changed from red to red-brown, and the insoluble $Ru_2(dpf)_4$ immediately dissolved. Nitrogen was then used to purge the solution until dry. The remaining solid left was washed using deaerated acetone several times to remove TBAP, and $Ru_2(dpf)_4(NO)_2$ was obtained with a yield of 99%. Crystals of $Ru_2(dpf)_4(NO)_2$ suitable for X-ray diffraction analysis were obtained by slow diffusion of hexanes into a CH_2Cl_2/benzene (98:2) solution of the compound. Anal. Calcd for $C_{52}H_{44}N_{10}O_2Ru_2$: C, 59.88; H, 4.25; N, 13.43. Found: C, 58.43; H, 3.91; N, 12.77. ^1H NMR (in CD_2Cl_2): δ 8.55 (s, 4H), 7.16 (t, 16H), 6.99 (t, 8H), 6.88 (d, 16H) ppm. Infrared spectrum (solid): 1747 (s), 1727 (s), 1592 (m), 1539 (s), 1486 (s), 1310 (m), 1215 (s) cm^{-1} (s, strong; m, medium). Mass spectral data [*m*/*e*, (fragment)]: 983 $[Ru_2(dpf)_4]^+$.

Synthesis of $[Ru_2(dpf)_4(NO)]^-$ or $[Ru_2(dpf)_4(NO)]^-TBA^+$ Bulk electrolysis of a CH_2Cl_2 solution of $Ru_2(dpf)_4(NO)$ containing 0.2 M TBAP was conducted in an open atmosphere at an applied potential of −0.20 V versus SCE. The color of the solution changed from green-blue to blood red gradually. When the current diminished significantly, the solution was then transferred into a flask, and a stream of nitrogen gas was applied to dry the solution which was then washed with absolute ethanol to remove the supporting electrolyte. UV−vis spectrum in CH_2Cl_2 [λ_{max}, nm]: 464, 510. Mass spectral data [*m*/*e*, (fragment)]: 983 $[Ru_2(dpf)_4]^+$. Infrared spectrum (solid): 1705 (s), 1593 (m), 1558 (s), 1485 (s), 1333 (m), 1222 (s) cm^{-1} (s, strong; m, medium). Attempts to grow a suitable single crystal for X-ray diffraction study were not successful.

X-ray Crystallography of $Ru_2(dpf)_4(NO)$ and $Ru_2(dpf)_4(NO)_2$. Single crystals of a green cube of $Ru_2(dpf)_4(NO)$ and a red-brown flaky plate of $Ru_2(dpf)_4(NO)_2$ were mounted on a Bruker SMART diffractometer for the former compound and on a Siemens SMART diffractometer for the latter one in a random orientation. The approximate dimensions of $Ru_2(dpf)_4(NO)$ and $Ru_2(dpf)_4(NO)_2$ were $0.11 \times 0.11 \times 0.11$ mm^3 and $0.20 \times 0.04 \times 0.01$ mm^3, respectively. The samples were placed in a stream of dry nitrogen gas at ambient temperature for $Ru_2(dpf)_4(NO)$ or at −54 °C for $Ru_2(dpf)_4(NO)_2$. Both diffractomers were equipped with a 1K CCD area detector, and the radiation used was Mo Kα (λ = 0.71073 Å) monochromatized by a highly ordered graphite crystal. A hemisphere of data (1271 frames at 5-cm detector distance) was collected using a narrow-frame method with scan widths of 0.30° in ω and an exposure time of 38 s/frame. The first 50 frames were remeasured at the end of data collection to monitor instrument and crystal stability, and the maximum correction on *I* was <1%.

The structure of $Ru_2(dpf)_4(NO)$ was solved using the direct methods program XS and difference Fourier maps and refined by using a full-matrix least-squares method. During data reduction, Lorentz and polarization corrections were applied. While these indicated a high degree of motion in the solvent molecule, no sensible disorder could be modeled. The data of $Ru_2(dpf)_4(NO)_2$ were integrated using the Siemens SAINT program, with the intensities corrected for Lorentz factor, polarization, air absorption, and absorption due to variation in the path-length through the detector faceplate. The structure was solved by direct methods and refined by full-matrix least-squares calculations on F^2. An absorption correction was applied on the entire data set using a Ψ-scan absorption correction program. A Ψ-scan absorption correction was applied based on the entire data set. Redundant reflections were reflections having $I > 10\sigma(I)$ for $Ru_2(dpf)_4(NO)$ and 1487 reflections having $I > 10\sigma(I)$ for $Ru_2(dpf)_4(NO)_2$. Anisotropic thermal parameters were refined for all non-hydrogen atoms. All calculations were made using the Siemens SHELXTL programs package. The Laue symmetry was determined to be 4/*mmm* for $Ru_2(dpf)_4(NO)$ and 2/*m* for $Ru_2(dpf)_4(NO)_2$, and from the systematic absences noted, the space group was shown to be *P*4/*ncc* for $Ru_2(dpf)_4(NO)$ and $P2_1/n$ for $Ru_2(dpf)_4(NO)_2$. Final cell constants as well as other information pertinent to data collection and structure refinement of $Ru_2(dpf)_4(NO)$ and $Ru_2(dpf)_4(NO)_2$ are listed in Table 1.

Table 1. Crystal Data and Data Collection and Processing Parameters for $Ru_2(dpf)_4(NO)$ and $Ru_2(dpf)_4(NO)_2$

	$Ru_2(dpf)_4(NO)$	$Ru_2(dpf)_4(NO)_2$
space group	*P*4/*ncc* tetragonal	$P2_1/n$ monoclinic
cell constant		
a (Å)	14.178(2)	12.1854(19)
b (Å)	14.178(5)	18.997(3)
c (Å)	23.734(5)	20.240(3)
β (deg)	90	101.197(3)
V (Å^3)	4770.8(13)	4596.2(13)
mol formula	$C_{52}H_{44}N_9ORu_2 \cdot C_3H_6O$	$C_{52}H_{44}N_{10}O_2Ru_2$
fw (g/mol)	1071.18	1043.11
Z	4	4
ρ_{calcd} (g/cm^3)	1.419	1.507
μ (mm^{-1})	0.69	0.711
λ(Mo Kα) (Å)	0.71073	0.71073
temp (K)	293	219
R (F_o)[a]	0.0428	0.0690
R_w (F_o)[b]	0.0833	0.0589

[a] $R = \sum||F_o| - |F_c||/\sum|F_o|$. [b] $R_w = [\sum_w(|F_o| - |F_c|)^2/\sum_w|F_o|^2]^{1/2}$.

Results and Discussion

Synthesis and Reaction Description. The reaction between $Ru_2(dpf)_4Cl$ and NO leads to $Ru_2(dpf)_4(NO)$ as the major product with a yield of 90%. There is no evidence to support formation of $Ru_2(dpf)_4(NO)Cl$ in either solution or the solid state as in the case when $Ru_2(Fap)_4(NO)Cl$ is formed in the reaction between NO and $Ru_2(Fap)_4Cl$.

The reaction between $Ru_2(dpf)_4Cl$ and NO was monitored electrochemically and is proposed to proceed as shown in eqs 1−2.

$$Ru_2(dpf)_4Cl + 2NO \rightarrow [Ru_2(dpf)_4(NO)_2]^+ + Cl^- \quad (1)$$

$$[Ru_2(dpf)_4(NO)_2]^+ \rightarrow Ru_2(dpf)_4(NO) + NO^+ \quad (2)$$

The assignment of $[Ru_2(dpf)_4(NO)_2]^+$ as an intermediate in the formation of $Ru_2(dpf)_4(NO)$ (eq 1) is based on the fact that the cyclic voltammograms of the reaction mixture closely resemble those of $[Ru_2(dpf)_4(NO)_2]^+$ which can be electrogenerated from $Ru_2(dpf)_4(NO)_2$ as described in the Electrochemistry section.

$[Ru_2(dpf)_4(NO)_2]^+$ formed in eq 1 is stable for several hours under N_2, but one NO^+ molecule is slowly lost to give the final mono-NO product, $Ru_2(dpf)_4(NO)$, as shown in eq

Table 2. Selected Bond Lengths (Å) and Bond Angles (deg) of Nitrosyl Diruthenium Complexes

	$Ru_2(dpf)_4(NO)$	$Ru_2(dpf)_4(NO)_2$	$Ru_2(EtCO_2)_4(NO)_2$[6]	$Ru_2(CF_3CO_2)_4(NO)_2$[6]	$Ru_2(Fap)_4(NO)Cl$[8]
			Bond Lengths (Å)		
Ru−Ru	2.4444(13)	2.6325(10)	2.515(4)	2.532(4)	2.4203(8)
Ru−N_L[a]	2.044[b]	2.099[b]			2.063
Ru−NO	1.809(11)	1.973[b]	1.781(7)	1.786(19)	1.869(6)
N−O	1.142(12)	1.156[b]	1.126(8)	1.121(24)	1.164(8)
			Bond Angles (deg)		
Ru−Ru−NO	180.00	173.15[b]	166.15[b]	168.41[b]	169.49(19)
Ru−N−O	180.00	162.35[b]	152.4(5)	152.2(21)	155.8(6)
Ru−Ru−N_L[a]	87.34[b]	83.68[b]			86.71

[a] Nitrogen of the bridging ligand (N_L). [b] Average values.

2. A similar loss of NO^+ occurs for $[Ru_2(dpf)_4(NO)_2]^+$ which can be generated electrochemically from $Ru_2(dpf)_4(NO)_2$.

The direct synthesis of $Ru_2(dpf)_4(NO)_2$ from $Ru_2(dpf)_4Cl$ and NO was not observed to occur, even with the use of excess NO gas or a prolonged reaction time. However, $Ru_2(dpf)_4(NO)_2$ was easily synthesized from $Ru_2(dpf)_4$ by purging NO gas into a CH_2Cl_2 solution of the Ru_2^{4+} complex which had been electrogenerated under an applied potential. A similar reaction route was used in the synthesis of $Ru_2(C_2H_5COO)_4(NO)_2$ and $Ru_2(CF_3COO)_4(NO)_2$.[6,8]

Both $Ru_2(dpf)_4(NO)$ and $Ru_2(dpf)_4(NO)_2$ are air stable in the solid state, and no dissociation of the axially bound NO was observed in air or under a vacuum created by a mechanical pump. $Ru_2(dpf)_4(NO)$ and $Ru_2(dpf)_4(NO)_2$ are both also air stable in solution under various experimental conditions, and no decomposition was observed, the only exception being for $Ru_2(dpf)_4(NO)_2$ in acetone.

Molecular Structures. Selected bond lengths and bond angles of $Ru_2(dpf)_4(NO)$ and $Ru_2(dpf)_4(NO)_2$ are summarized in Table 2 along with the bond lengths and bond angles of earlier characterized nitrosyl diruthenium complexes. The molecular structures of $Ru_2(dpf)_4(NO)$ and $Ru_2(dpf)_4(NO)_2$ are illustrated in Figure 1. All intramolecular bond lengths and bond angles as well as other structural data of these compounds are given in the Supporting Information.

The coordinations about Ru1 and Ru2 in $Ru_2(dpf)_4(NO)$ are essentially octahedral and square pyramidal, respectively, with four dpf nitrogens in each of the equatorial planes with a C_{4v} symmetry and a NO molecule coordinated to Ru1 (Figure 1a). In $Ru_2(dpf)_4(NO)_2$, the coordinations about Ru1 and Ru2 are essentially octahedral with four nitrogens of the dpf ligands forming the equatorial plane and each ruthenium atom bound to one NO molecule (Figure 1b).

The Ru−Ru bond distances of $Ru_2(dpf)_4(NO)$ and $Ru_2(dpf)_4(NO)_2$ are 2.4444(13) and 2.6325(10) Å, respectively, and these values are within the expected range of Ru−Ru bond distances of other diruthenium complexes.[5,11,16,18] As shown in Table 2, the Ru−Ru bond distance increases from 2.4444(13) to 2.6325(10) Å upon going from the mono-NO to the bis-NO dpf complex. This elongation is attributed to the fact that the metal−metal bond order is decreased from 1.5 in $Ru_2(dpf)_4(NO)$ to 1.0 in $Ru_2(dpf)_4(NO)_2$. It should be noted that the formal oxidation states are proposed to be Ru_2^{3+} for $Ru_2(dpf)_4(NO)$ and Ru_2^{2+} for $Ru_2(dpf)_4(NO)_2$, respectively (see next sections). The Ru−Ru bond length of $Ru_2(dpf)_4(NO)$ is also in the range of other structurally characterized nitrosyl complexes; however, the Ru−Ru bond distance of $Ru_2(dpf)_4(NO)_2$ is the longest metal−metal bond length of all the known nitrosyl diruthenium complexes (see Table 2).

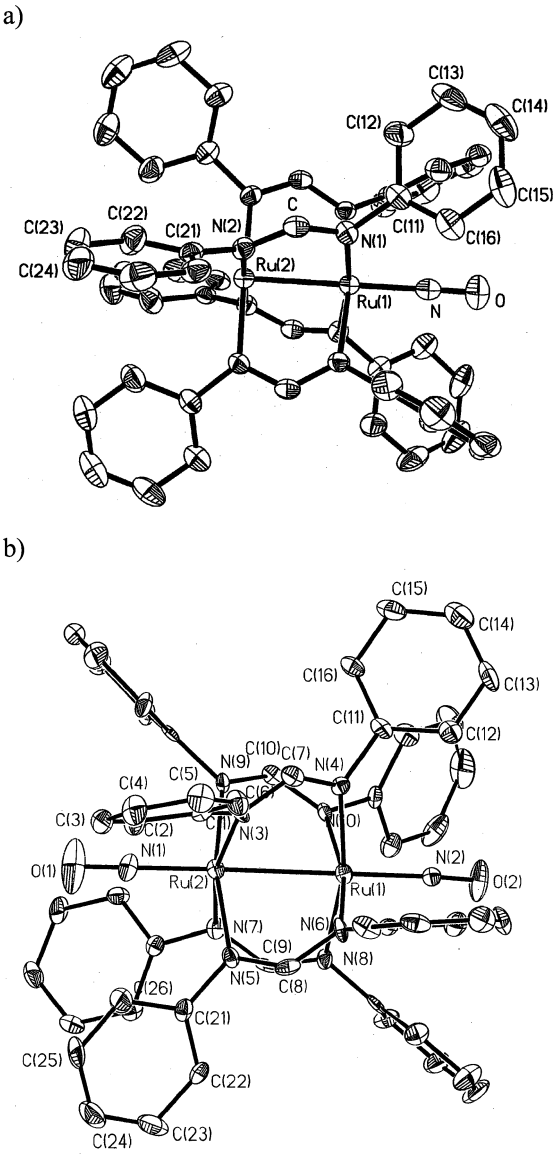

Figure 1. Thermal ellipsoid plot (30% equiprobability envelopes) of (a) $Ru_2(dpf)_4(NO)$ and (b) $Ru_2(dpf)_4(NO)_2$. Hydrogen atoms have been omitted for clarity.

(18) Xu, G.-L.; Jablonski, C. G.; Ren, T. *Inorg. Chim. Acta* **2003**, *343*, 387−390.

The metal−metal bond distance in diruthenium complexes having NO axial ligands greatly depends on the type of equatorial bridging ligands. For instance, the Ru−Ru bond length increases from 2.5125(4) to 2.6325(10) Å upon going from $Ru_2(EtCO_2)_4(NO)_2$ to $Ru_2(dpf)_4(NO)_2$.

As shown in Table 2, the Ru−NO bond length significantly increases from 1.809(11) to 1.973 Å upon going from $Ru_2(dpf)_4(NO)$ to $Ru_2(dpf)_4(NO)_2$. The Ru−NO bond distance of $Ru_2(dpf)_4(NO)$ (1.809(11) Å) is slightly longer than those reported for $Ru_2(EtCO_2)_4(NO)_2$ and $Ru_2(CF_3CO_2)_4(NO)_2$ but is shorter than those of $Ru_2(dpf)_4(NO)_2$ and $Ru_2(Fap)_4(NO)Cl$. The N−O bond distances of both $Ru_2(dpf)_4(NO)$ and $Ru_2(dpf)_4(NO)_2$ are within the range 1.121−1.164 Å for other reported nitrosyl diruthenium complexes (Table 2).

The Ru−Ru−NO and Ru−N−O bond angles decrease upon going from $Ru_2(dpf)_4(NO)$ to $Ru_2(dpf)_4(NO)_2$ as shown in Table 2, but both bond angles are greater than that reported for $Ru_2(Fap)_4(NO)Cl$. This result could be explained in terms of the different types of bridging ligands (dpf vs Fap). The Ru−N−O bond angles of $Ru_2(dpf)_4(NO)$ and $Ru_2(dpf)_4(NO)_2$ are 180° and 162.35°, respectively, and those values are comparable to other reported nitrosyl diruthenium complexes (see Table 2) even though the values of the dpf complexes are much higher. It should be noted that the Ru−N−O bond angle of 152.4(5)° in $Ru_2(EtCO_2)_4(NO)_2$ is still considered to be linear.[11]

The framework of the dpf ligand seems to remain unchanged upon going from the mono-NO to bis-NO diruthenium complexes as shown in Table 2. For example, the average $Ru-N_L$ bond distance in $Ru_2(dpf)_4(NO)$ is 2.044 Å and that of $Ru_2(dpf)_4(NO)_2$ is 2.099 Å. Also, the Ru−Ru−N_L bond angle is only slightly decreased from 87.34° for $Ru_2(dpf)_4(NO)$ to 83.68° for $Ru_2(dpf)_4(NO)_2$. This result is consistent with what has been reported for dpf complexes upon going from the mono-axial ligand to bis-axial ligands.[15]

Electronic Configurations. $Ru_2(dpf)_4(NO)$ contains three unpaired electrons as evidenced by the fact that the compound has a room-temperature magnetic moment of 4.01 μ_B. The lack of an ESR and NMR signals is also consistent with what has been reported for Ru_2 complexes having three unpaired electrons which show no signal at all or ill-resolved ESR spectra.[19,20] The lack of a characteristic ESR signal attributed to NO also indicates that there is not an unpaired electron located on the NO axial ligand.[21−23]

The formal oxidation state of the Ru_2 core in $Ru_2(dpf)_4(NO)$ is assigned as Ru_2^{3+} on the basis of previous assignments for other reported nitrosyl diruthenium complexes where the NO ligand donates its odd π^*-electron to the Ru_2 core.[6,8] The ground-state electronic configuration of $Ru_2(dpf)_4(NO)$ is therefore proposed to be $(\sigma)^2(\pi)^4(\delta)^2(\delta^*)^2(\pi^*)^2(\sigma^*)^1$.

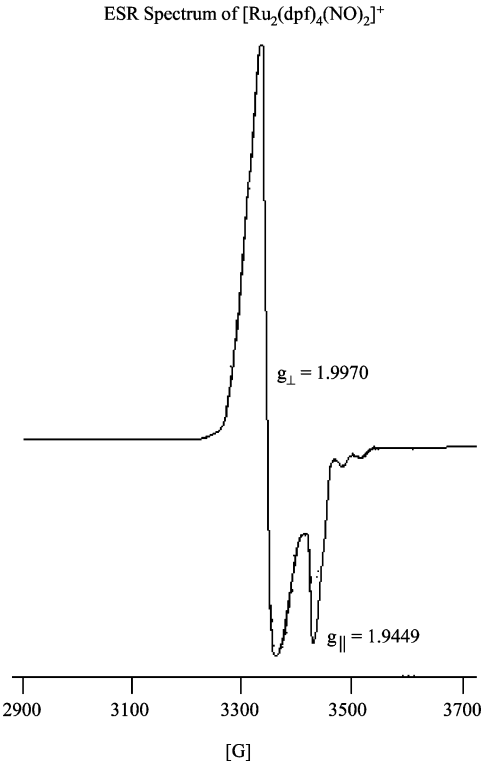

Figure 2. ESR spectrum of electrochemically generated $[Ru_2(dpf)_4(NO)_2]^+$ by bulk electrolysis at 0.6 V vs SCE in CH_2Cl_2, 0.1 M TBAP under N_2.

In contrast to the mono-NO adduct, $Ru_2(dpf)_4(NO)_2$ is diamagnetic as confirmed by its well-resolved ^1H NMR signals. This compound is believed to have a formal oxidation state of Ru_2^{2+}, where each NO ligand donates its odd π^*-electron to the Ru_2 core, giving a ground-state electronic configuration of $(\sigma)^2(\pi)^4(\delta)^2(\pi^*)^4(\delta^*)^2$. Finally, the isolated singly reduced species, $[Ru_2(dpf)_4(NO)]^-$, is also paramagnetic (no ESR or NMR spectrum) with $(\sigma)^2(\pi)^4(\delta)^2(\delta^*)^2(\pi^*)^3(\sigma^*)^1$ being proposed as its electron configuration in the ground state.

The ESR signal of $[Ru_2(dpf)_4(NO)_2]^+$ generated after controlled-potential oxidation of $Ru_2(dpf)_4(NO)_2$ in CH_2Cl_2, 0.2 M TBAP under N_2, shows a signal with $g_\perp = 1.9970$ and $g_{||} = 1.9449$ (Figure 2). The shape of the ESR signal is consistent with a species having a single unpaired electron rather than three unpaired electrons, a condition under which either no ESR spectrum or a broad and ill-resolved ESR spectrum should be obtained.[7,8,15,24]

There are two possible sites to abstract an electron from the antibonding orbitals in $Ru_2(dpf)_4(NO)_2$, π^* or δ^*. In the first case, the electronic configuration would be $(\sigma)^2(\pi)^4(\delta)^2(\delta^*)^2(\pi^*)^3$, and in the second case, it would be $(\sigma)^2(\pi)^4(\delta)^2(\pi^*)^4(\delta^*)^1$. The first electronic configuration has a ground state which possesses an orbitally degenerate ^2E_g state, which would result in extremely fast relaxation and signal broadening.[15,19,24] This is not observed for $[Ru_2(dpf)_4(NO)_2]^+$, where a sharp and well-resolved signal is seen, suggesting a ground-state electronic configuration of $(\sigma)^2(\pi)^4(\delta)^2(\pi^*)^4(\delta^*)^1$. In this configuration, only one electron occupies the δ^* orbital rather than having three electrons reside in the π^* orbital to

(19) Cotton, F. A.; Pedersen, E. *Inorg. Chem.* **1975**, *14*, 388.
(20) Bear, J. L.; Li, Y.; Han, B.; Van Caemelbecke, E.; Kadish, K. M. *Inorg. Chem.* **1997**, *36*, 5449.
(21) Jarke, F. H.; Ashford, N. A.; Solomon, I. J. *J. Chem. Phys.* **1976**, *64*, 3097.
(22) Wayland, B. B.; Newman, A. R. *Inorg. Chem.* **1981**, *20*, 3093.
(23) Yoshimura, T. *Inorg. Chem.* **1986**, *25*, 688.
(24) Bear, J. L.; Han, B.; Huang, S. *J. Am. Chem. Soc.* **1993**, *115*, 1175.

Table 3. Magnetic Properties and Proposed Electronic Configurations of Several Diruthenium Complexes

compd	formal oxidn state	Ru−Ru (Å)	no. unpaired electrons	electronic configuration	ref[a]
$Ru_2(dpf)_4Cl$	Ru_2^{5+}	2.339(1)	3	$\sigma^2\pi^4\delta^2\pi^{*2}\delta^{*1}$	15
$Ru_2(dpf)_4(CO)$	Ru_2^{4+}	2.5544(8)	0	$\sigma^2\pi^4\delta^2\pi^{*4}$	7
$[Ru_2(dpf)_4(NO)_2]^+$	Ru_2^{3+}		1	$\sigma^2\pi^4\delta^2\pi^{*4}\delta^{*1}$	tw
$[Ru_2(dpf)_4(CO)]^-$	Ru_2^{3+}		1	$\sigma^2\pi^4\delta^2\pi^{*4}\delta^{*1}$	7
$Ru_2(dpf)_4(NO)$	Ru_2^{3+}	2.4444(13)	3	$\sigma^2\pi^4\delta^2\delta^{*2}\pi^{*2}\sigma^{*1}$	tw
$[Ru_2(dpf)_4(NO)]^-$	Ru_2^{2+}		2	$\sigma^2\pi^4\delta^2\delta^{*2}\pi^{*3}\sigma^{*1}$	tw
$Ru_2(dpf)_4(NO)_2$	Ru_2^{2+}	2.6325(10)	0	$\sigma^2\pi^4\delta^2\delta^{*2}\pi^{*4}$	tw
$Ru_2(Fap)_4(NO)Cl$	Ru_2^{4+}	2.4203(8)	2	$\sigma^2\pi^4\delta^2\pi^{*3}\delta^{*1}$	8
$Ru_2(EtCO_2)_4(NO)_2$	Ru_2^{2+}	2.515(4)	0	$\sigma^2\pi^4\delta^2\pi^{*4}\delta^{*2}$	6
$Ru_2(CF_3CO_2)_4(NO)_2$	Ru_2^{2+}	2.532(4)	0	$\sigma^2\pi^4\delta^2\pi^{*4}\delta^{*2}$	6

[a] tw = this work.

Table 4. Half-Wave Potentials (V vs SCE) of Diruthenium Complexes under N_2 unless Otherwise Indicated

compd	formal oxidn state	axial ligand L_1	axial ligand L_2	solution condition[a]	$E_{1/2}$ (V vs SCE) 2nd oxidn	1st oxidn	1st redn	2nd redn	ref
$Ru_2(dpf)_4Cl$	Ru_2^{5+}	Cl		CH_2Cl_2, TBAP		0.54	−0.64[f]		15
$Ru_2(dpf)_4(CO)$	Ru_2^{4+}	CO		CH_2Cl_2, TBAP		0.28	−1.17		7
				CH_2Cl_2, TBAP, CO atm		0.28	−1.07	−1.79	7
$Ru_2(dpf)_4(NO)$	Ru_2^{3+}	NO		CH_2Cl_2, TBABr[b]			0.06	−1.24	tw
				CH_2Cl_2, TBABr, CO atm			0.18	−0.78	tw
$[Ru_2(dpf)_4(NO)]^-$	Ru_2^{2+}	NO		CH_2Cl_2, TBAP[c]		0.02	−1.28		tw
$[Ru_2(dpf)_4(NO)(CO)]^-$	Ru_2^{2+}	NO	CO	CH_2Cl_2, TBAP[d]		0.15	−0.82		tw
$Ru_2(dpf)_4(NO)_2$	Ru_2^{2+}	NO	NO	CH_2Cl_2, TBAP	1.15	0.24	−1.24	−1.96[f]	tw
$Ru_2(Ph_2N_3)_4(NO)_2$	Ru_2^{2+}	NO	NO	CH_2Cl_2, $TBAPF_6$[e]	1.33	0.54	−0.95	−1.75	6
$Ru_2(EtCO_2)_4(NO)_2$	Ru_2^{2+}	NO	NO	CH_2Cl_2, $TBAPF_6$[e]		1.15	−0.86[f]		6
$Ru_2(Fap)_4(NO)Cl$	Ru_2^{4+}	NO	Cl	CH_2Cl_2, TBAP		1.14	−0.03	−1.27	8

[a] Supporting electrolyte concentration = 0.1 M unless otherwise noted. [b] In CH_2Cl_2, 0.1 M TBAP, $E_{1/2}$ = 0.02 and −1.29 V. In PhCN, 0.1 M TBAP, $E_{1/2}$ = 0.04 and −1.18 V. [c] In PhCN, 0.1 M TABP, $E_{1/2}$ = 0.02 and −1.21 V. [d] In PhCN, 0.1 M TBAP, $E_{1/2}$ = 0.15 and −0.76 V. [e] 0.2 M. [f] E_{pc} value. tw = this work.

give an $S = {}^1/_2$ system.[7,8,15,24] The magnetic properties and the proposed electronic configurations of selected diruthenium complexes are summarized in Table 3.

The appearance of hyperfine splitting on the $g_{||}$ tensor in Figure 2 has been addressed in the literature for Ru_2 complexes bridged by dpf ligands and is known to result from different nuclear spin constants of the ruthenium isotopes which are present in the radical cation complex.[15,24] No ^{14}N hyperfine splitting was seen in the ESR spectrum of singly oxidized $Ru_2(dpf)_4(NO)_2$, thus suggesting that the oxidation of $Ru_2(dpf)_4(NO)_2$ occurs on the diruthenium core and not on the NO ligand. A similar assignment can also be proposed on the basis of FTIR-spectroelectrochemical measurements.

Electrochemistry. Cyclic voltammograms of $Ru_2(dpf)_4(NO)$ and $Ru_2(dpf)_4(NO)_2$ in CH_2Cl_2 under N_2 and CO are shown in Figure 3, and half-wave potentials along with data for oxidation or reduction of related diruthenium complexes are given in Table 4.

As shown in Figure 3a and Table 4, $Ru_2(dpf)_4(NO)$ undergoes two reversible one-electron reductions at $E_{1/2}$ = 0.06 and −1.24 V versus SCE in CH_2Cl_2, 0.1 M TBABr under N_2. These processes are positively shifted to $E_{1/2}$ = 0.18 and −0.78 V under CO, resulting from trans-coordination of a CO molecule which stabilizes the singly and doubly reduced metal−metal bonded complexes, thus leading to easier reductions.

The two reversible one-electron reductions of $Ru_2(dpf)_4(NO)$ under N_2 are metal-centered and correspond to formation of diruthenium complexes with formal oxidation states

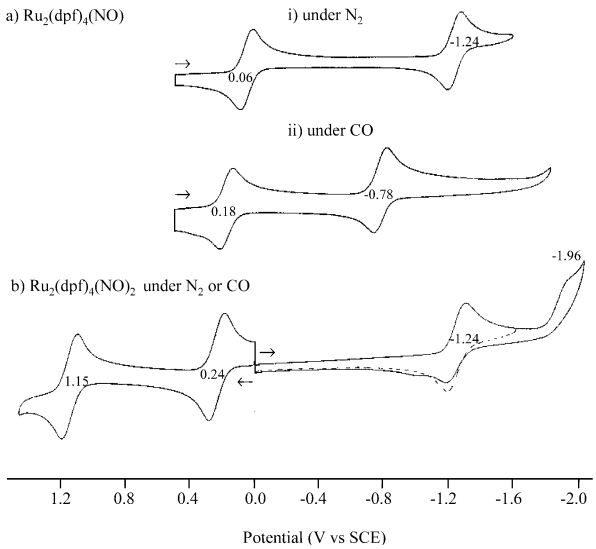

Figure 3. Cyclic voltammograms of (a) $Ru_2(dpf)_4(NO)$ (i) under N_2 or (ii) under CO in CH_2Cl_2, 0.1 M TBABr, and (b) $Ru_2(dpf)_4(NO)_2$ under either N_2 or CO in CH_2Cl_2, 0.1 M TBAP. Scan rate = 0.1 V/s.

of Ru_2^{2+} and Ru_2^{1+}, respectively. Both reduction processes of $Ru_2(dpf)_4(NO)$ under CO are also assigned as being metal-centered on the basis of the infrared spectral data.

The infrared and UV−vis data of neutral $Ru_2(dpf)_4(NO)$ are the same under N_2 and CO (see next sections), thus indicating that a CO molecule is not axially coordinated to the Ru_2 core. However, the cyclic voltammograms of $Ru_2(dpf)_4(NO)$ are different under N_2 and CO atmospheres, and the difference in redox potential between the two conditions

indicates that a CO molecule binds to the singly reduced species which is generated after the first reduction of $Ru_2(dpf)_4(NO)$ to yield $[Ru_2(dpf)_4(NO)(CO)]^-$ in solution. The $E_{1/2}$ value for the first reduction of $Ru_2(dpf)_4(NO)$ under CO is 120 mV more positive than for the same compound under N_2, and this compares to a 100 mV difference in $E_{1/2}$ for reduction of $Ru_2(dpf)_4CO$ under a N_2 or CO atmosphere in CH_2Cl_2 where $[Ru_2(dpf)_4(CO)_2]^-$ is the final electrogenerated product under CO.[7] The second reduction of $Ru_2(dpf)_4(NO)$ under CO ($E_{1/2} = -0.78$ V) is also much easier than that of the same compound under N_2 ($E_{1/2} = -1.24$ V), and this is consistent with CO stabilization of the lower oxidation state.[7,9]

To our knowledge, this is the only example of a diruthenium complex with both NO and CO as axial ligands, thus providing us with an opportunity to study by means of infrared spectroelectrochemistry the interaction between NO and CO across the Ru−Ru bond.

Changing the axial ligand from CO to NO significantly alters the electrochemistry of the Ru_2 core containing a dpf bridging ligand. For example, the first reduction of $Ru_2(dpf)_4(NO)$ under N_2 occurs at $E_{1/2}$ at 0.06 V (Table 4), but this reduction is shifted negatively by 1.23 V for $Ru_2(dpf)_4(CO)$.[7] The two reductions of $Ru_2(dpf)_4(NO)$ under N_2 are, however, comparable to those of $Ru_2(Fap)_4(NO)Cl$[8] where $E_{1/2} = -0.03$ and -1.27 V in CH_2Cl_2 containing 0.1 M TBAP.[8]

As shown in Figure 3b and Table 4, $Ru_2(dpf)_4(NO)_2$, which formally contains a Ru_2^{2+} center, undergoes a reversible one-electron reduction at $E_{1/2} = -1.24$ V versus SCE and an irreversible reduction at $E_{pc} = -1.96$ V in CH_2Cl_2, 0.1 M TBAP under N_2. The irreversible features of the second reduction are believed to be due to a cleavage of the M−NO bond on the cyclic voltammetry time scale.

The two reversible one-electron oxidations of $Ru_2(dpf)_4(NO)_2$ ($E_{1/2} = 0.24$ and 1.15 V) correspond to formation of diruthenium complexes with formal oxidation states of Ru_2^{3+} and Ru_2^{4+}, respectively. The electrochemical properties of the bis-NO diruthenium complexes also depend on the type of bridging ligands. For example, the first oxidation of $Ru_2(dpf)_4(NO)_2$ is located at $E_{1/2} = 0.24$ V in CH_2Cl_2 containing 0.1 M TBAP (Table 4), but this half-wave potential is positively shifted by 0.91 V for $Ru_2(EtCO_2)_4(NO)_2$ in CH_2Cl_2, 0.2 M $TBAPF_6$.[6] However, the two oxidations of $Ru_2(dpf)_4(NO)_2$ are comparable to those of $Ru_2(Ph_2N_3)_4(NO)_2$ in CH_2Cl_2, 0.2 M $TBAPF_6$ (Table 4).[6]

It should be noted that no shifts in half-wave potentials for oxidation or reduction of $Ru_2(dpf)_4(NO)_2$ are seen upon changing from a N_2 to a CO atmosphere, thus indicating the absence of CO binding to the neutral, electro-oxidized, or electroreduced products.

Analysis of NO and CO Interaction. The infrared spectrum of $Ru_2(dpf)_4(NO)$ in CH_2Cl_2, 0.2 M TBABr, is characterized by a single NO stretching vibration at $\nu_{NO} = 1786$ cm^{-1} independent of the gas above the solution (N_2 or CO) as shown in Figure 4a. This value is higher than the ν_{NO} of 1740 cm^{-1} for $Ru_2(Fap)_4(NO)Cl$ or 1745 cm^{-1} for $Ru_2(EtCO_2)_4(NO)_2$, consistent with the more linear Ru−N−O bond angle in $Ru_2(dpf)_4(NO)$ (179.9°) as compared to $Ru_2(Fap)_4(NO)Cl$ (155.8°) or $Ru_2(EtCO_2)_4(NO)_2$ (152.4°).[6,8] These values and those of other diruthenium complexes with NO or CO axial ligands are summarized in Table 5.

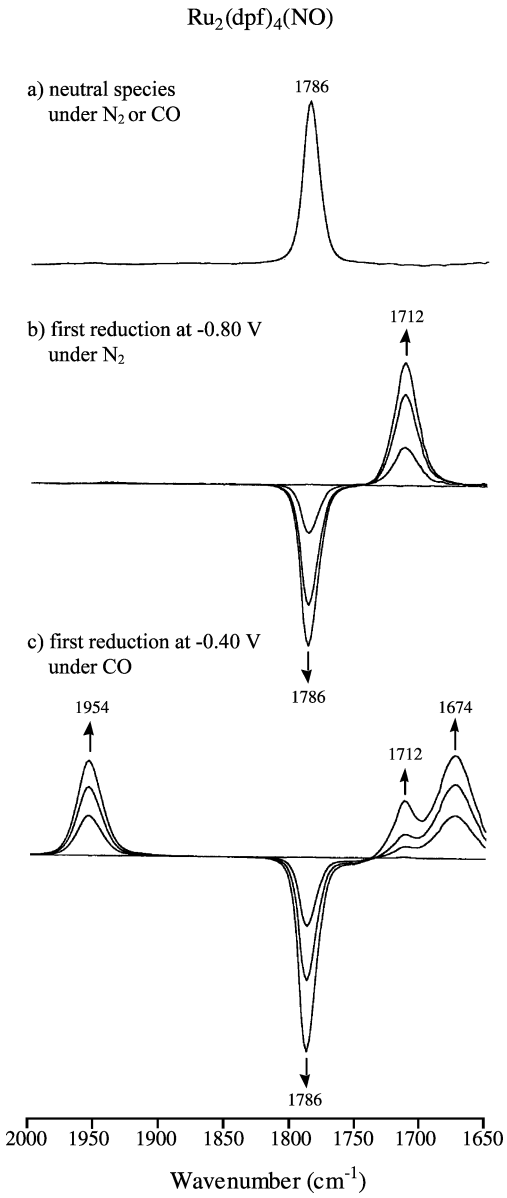

Figure 4. Thin-layer FTIR spectral changes of $Ru_2(dpf)_4(NO)$ for (a) neutral species under N_2 or CO, (b) during first reduction under N_2, and (c) during first reduction under CO in CH_2Cl_2, 0.2 M TBABr.

The fact that ν_{NO} for $Ru_2(dpf)_4(NO)$ is the same under N_2 or CO, along with the absence of any CO stretching vibration for the compound under CO, clearly indicates that CO does not bind to $Ru_2(dpf)_4(NO)$ in its neutral form. This result is also self-consistent with results from the electrochemical studies.

As shown in Figure 4b and Table 5, the ν_{NO} value of 1786 cm^{-1} for $Ru_2(dpf)_4(NO)$ is shifted to a lower frequency of 1712 cm^{-1} upon the addition of one electron under N_2 to generate $[Ru_2(dpf)_4(NO)]^-$. This 74 cm^{-1} shift in the NO stretching vibration is comparable to a 71 cm^{-1} shift reported in the literature after the one-electron reduction of $Ru_2(Fap)_4(NO)Cl$.[8] The $\Delta\nu_{NO}$ of 74 cm^{-1} is also comparable to the

Table 5. Infrared (in CH_2Cl_2) and UV−Vis Spectral (in CH_2Cl_2 or PhCN) Data of Diruthenium Complexes[a]

compd	formal oxidn state	axial ligand		stretching frequency, cm^{-1}		λ_{max}, nm	ref[b]
		L_1	L_2	ν_{NO}	ν_{CO}		
$Ru_2(dpf)_4Cl$	Ru_2^{5+}	Cl				465, 570[c]	15
$Ru_2(dpf)_4(CO)$	Ru_2^{4+}	CO			1929	423, 526, 615[c]	7
$[Ru_2(dpf)_4(CO)]^-$	Ru_2^{3+}	CO			1840		7
$Ru_2(dpf)_4(NO)$	Ru_2^{3+}	NO		1786		455, 690[d]	tw
$[Ru_2(dpf)_4(NO)]^-$	Ru_2^{2+}	NO		1712		464, 510[d]	tw
$[Ru_2(dpf)_4(NO)]^{2-}$		NO		not observed		512[d]	tw
$[Ru_2(dpf)_4(CO)_2]^-$		CO	CO		1842		7
$[Ru_2(dpf)_4(NO)(CO)]^-$	Ru_2^{2+}	NO	CO	1674	1954	425, 565[d]	tw
$[Ru_2(dpf)_4(NO)(CO)]^{2-}$		NO	CO	1736	1909		tw
$Ru_2(dpf)_4(NO)_2$	Ru_2^{2+}	NO	NO	1726		345[c]	tw
$[Ru_2(dpf)_4(NO)_2]^+$	Ru_2^{3+}	NO	NO	1788		447, 785[c]	tw
$[Ru_2(dpf)_4(NO)_2]^{2+}$		NO	NO	1834		638, 920[c]	tw
$Ru_2(Fap)_4(NO)Cl$	Ru_2^{4+}	NO	Cl	1740		452, 687[c]	8
$[Ru_2(Fap)_4(NO)Cl]^-$	Ru_2^{3+}	NO	Cl	1669			8
$Ru_2(EtCO_2)_4(NO)_2$	Ru_2^{2+}	NO	NO	1745			6
$Ru_2(CF_3CO_2)_4(NO)_2$	Ru_2^{2+}	NO	NO	1800			6

[a] Anionic complexes are electrogenerated. [b] tw = this work. [c] In CH_2Cl_2. [d] In PhCN.

shift in CO stretching vibrations of 65−89 cm^{-1} upon the one-electron reduction of $[Ru_2(L)_4(CO)]$, where L is dpf[7] or a substituted ap ligand[9] (ap = 2-anilinopyridinate). The red shift in ν_{NO} upon reduction can be accounted for by an increased electron density on the Ru_2 core when $Ru_2(dpf)_4$-(NO) is reduced by one electron, thus leading to a stronger back-donation from the Ru_2 core to the antibonding π^* orbital.

Upon the second reduction of $Ru_2(dpf)_4(NO)$ under N_2, the NO vibration band at 1712 cm^{-1} disappears, and no clear NO stretching vibration band can be seen within the IR window (2000−1650 cm^{-1}). This result can be accounted for by a more increased electron density on the Ru_2 core, causing the NO vibration band to shift to a frequency lower than 1650 cm^{-1} where interference from overlapping absorbances of the solvent and supporting electrolyte prevents measurement of any NO bands in this region.

Thin-layer FTIR spectra obtained during the first reduction of $Ru_2(dpf)_4(NO)$ under CO in CH_2Cl_2, 0.2 M TBABr, are illustrated in Figure 4c and show the disappearance of the NO band at 1786 cm^{-1} along with the appearance of two new bands at 1674 and 1954 cm^{-1}. The first band is assigned to ν_{NO} and the second to ν_{CO} (Figure 4c and Table 5). The infrared spectra and electrochemical data are thus self-consistent, and both agree with the fact that a single CO molecule binds to $[Ru_2(dpf)_4(NO)]^-$ after the first reduction to generate $[Ru_2(dpf)_4(NO)(CO)]^-$, a diruthenium species containing both NO and CO axial ligands.

A red shift of 38 cm^{-1} in ν_{NO} is observed upon going from $[Ru_2(dpf)_4(NO)]^-$ to $[Ru_2(dpf)_4(NO)(CO)]^-$ and results from enhancement of the π-back-donation from the diruthenium metal centers to the NO ligand upon coordination of a CO molecule. The CO stretching vibrations in $Ru_2(dpf)_4(CO)$ and $[Ru_2(dpf)_4(CO)]^-$ are located at 1929 and 1840 cm^{-1}, respectively, under N_2, suggesting that the ν_{CO} at 1954 cm^{-1} for $[Ru_2(dpf)_4(NO)(CO)]^-$ results from a weaker π-back-donation from the Ru_2 core to the CO ligand.[7] The small peak at 1712 cm^{-1} in Figure 4c is due to a NO vibration of the complex without bound CO (Figure 4b), owing to low CO partial pressures above the CH_2Cl_2 solution.

The fact that ν_{NO} and ν_{CO} shift in an opposite direction upon the one-electron reduction of $[Ru_2(dpf)_4(NO)(CO)]^-$ suggests that the bound CO acts as an electron donor while the bound NO is the electron acceptor. This provides clear evidence for the existence of a strong interaction between axially bound NO and CO across the Ru−Ru bond.

The peaks at 1674 and 1954 cm^{-1} for $[Ru_2(dpf)_4(NO)(CO)]^-$ diminish, and two new peaks at 1736 and 1909 cm^{-1} appear upon electrogeneration of $[Ru_2(dpf)_4(NO)(CO)]^{2-}$ in CH_2Cl_2, 0.1 M TBABr under CO (see Table 5). The peak at 1909 cm^{-1} is assigned as the CO stretching vibration in the doubly reduced species while the peak at 1736 cm^{-1} is most likely due to ν_{NO}.

The NO stretching vibration frequencies of bis-NO diruthenium complexes should depend on the type of bridging ligands. $Ru_2(dpf)_4(NO)_2$ has a single ν_{NO} band at 1726 cm^{-1} in CH_2Cl_2, 0.1 M TBAP under N_2, while ν_{NO} is located at 1800 cm^{-1} for $Ru_2(CF_3CO_2)_4(NO)_2$ in CH_2Cl_2 without supporting electrolyte.[6] This difference in ν_{NO} could be due to the different electron densities on the Ru_2 core in the two complexes.

When $Ru_2(dpf)_4(NO)_2$ is converted to $[Ru_2(dpf)_4(NO)_2]^+$ in the FTIR cell, the ν_{NO} band at 1726 cm^{-1} disappears while a new NO band appears at 1788 cm^{-1} (Table 5). This 62 cm^{-1} blue-shift results from a weakened back-donation from the Ru_2 core to the antibonding π^* orbital of NO and is consistent with decreased electron density on the diruthenium core. The spectral changes are reversible, and the IR spectrum of $Ru_2(dpf)_4(NO)_2$ could be regenerated upon re-reduction at a controlled potential. Electro-oxidized $[Ru_2(dpf)_4(NO)_2]^+$ is stable on the experimental time scale of cyclic voltammetry (several seconds), and the NO group remains bound to the complex after the first oxidation.

The NO stretching vibration band of doubly oxidized $[Ru_2(dpf)_4(NO)_2]^{2+}$ appears at 1834 cm^{-1} in the same solution (Table 5). These spectral changes are not reversible, suggesting that the doubly oxidized complex is not stable on the experimental time scale.

Additional Characterization of $[Ru_2(dpf)_4(NO)(CO)]^-$. To further examine and confirm the interaction between NO

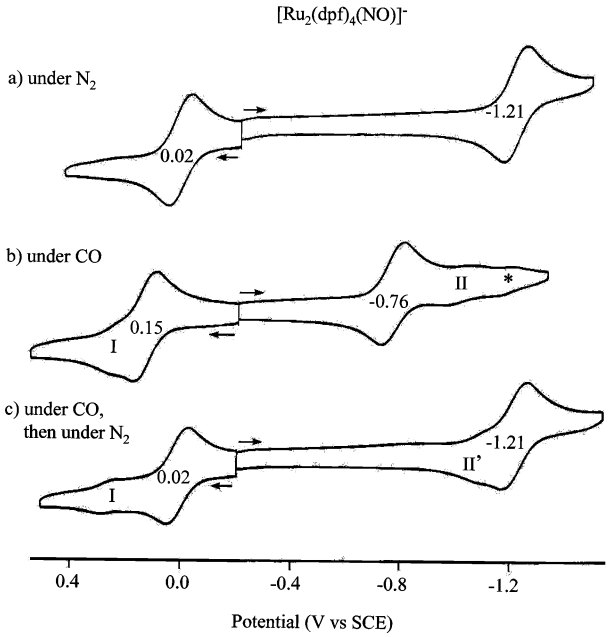

Figure 5. Cyclic voltammograms of $[Ru_2(dpf)_4(NO)]^-$ (a) under N_2, (b) under CO, and (c) under CO, then N_2 in PhCN, 0.1 TBAP. Scan rate = 0.1 V/s. Asterisk (*) assigned as unreacted $[Ru_2(dpf)_4(NO)]^-$ while reactions I and II are due to $Ru_2(dpf)_4(CO)$.

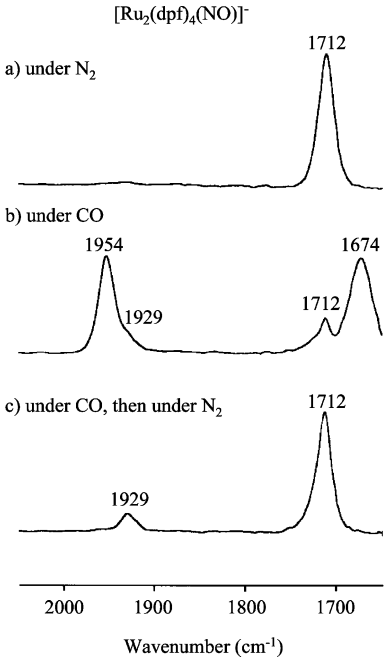

Figure 6. FTIR spectra of $[Ru_2(dpf)_4(NO)]^-$ (a) under N_2, (b) under CO, and (c) under CO, then N_2, in CH_2Cl_2. Peak at 1929 cm^{-1} due to trace $Ru_2(dpf)_4(CO)$ formed under CO.

and CO across the Ru−Ru bond, the electrochemical and spectroscopic properties of $[Ru_2(dpf)_4(NO)]^-$ were investigated under N_2 and CO atmospheres.

$[Ru_2(dpf)_4(NO)]^-$ undergoes a reversible one-electron oxidation at $E_{1/2} = 0.02$ V and a reversible one-electron reduction at $E_{1/2} = -1.21$ V in PhCN containing 0.1 M TBAP under N_2. Under a CO atmosphere, these $E_{1/2}$ values are positively shifted to 0.15 and −0.76 V, respectively (Figure 5). Identical shifts in half-wave potentials are obtained for $Ru_2(dpf)_4(NO)$ under N_2 and CO (see Figure 3 and Table 4).

The appearance of processes I and II in Figure 5b,c is due to the formation of $Ru_2(dpf)_4(CO)$ from $[Ru_2(dpf)_4(NO)]^-$ under CO. These processes are reversible and located at $E_{1/2} = 0.28$ and −1.07 V, respectively, in CH_2Cl_2, 0.1 M TBAP under CO, as reported in the literature for oxidation and reduction of $Ru_2(dpf)_4(CO)$.[7]

Wave I in Figure 5b remains unchanged upon going from CO to N_2 above the solution while wave II shifts negatively to $E_{1/2} = -1.15$ V (labeled II′) after removal of CO by N_2. This is consistent with the electrochemical behavior of $Ru_2(dpf)_4(CO)$ under CO and N_2.[7]

Scheme 1. Overall Electron Transfer Processes and Chemical Reactions of the Investigated Nitrosyl Diruthenium Complexes, Where dpf Is the *N*,*N*-diphenylformamidinate Anion

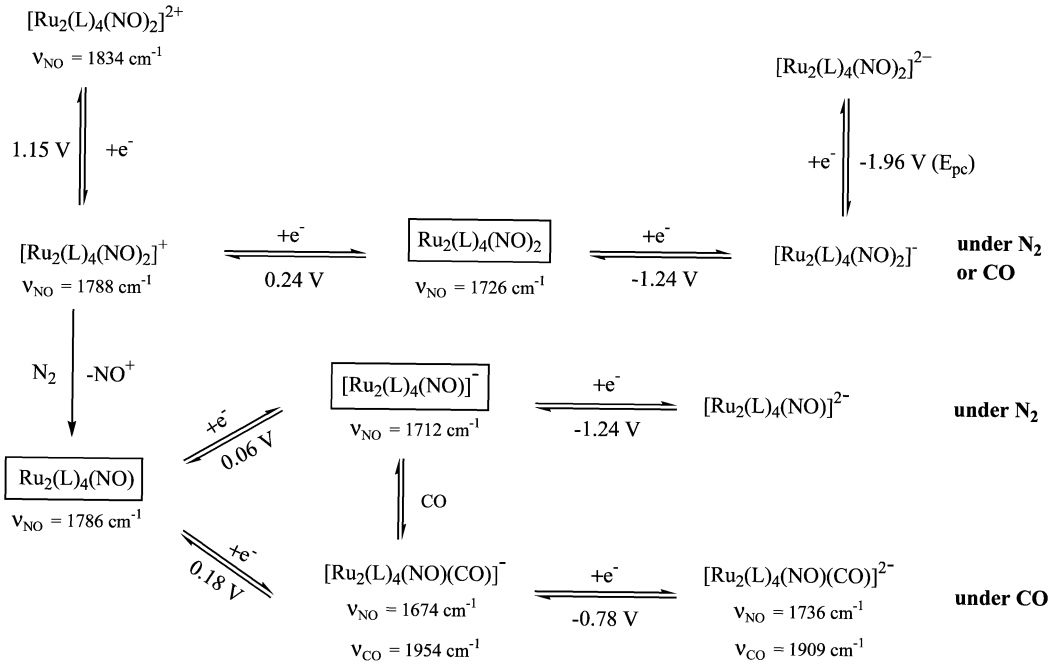

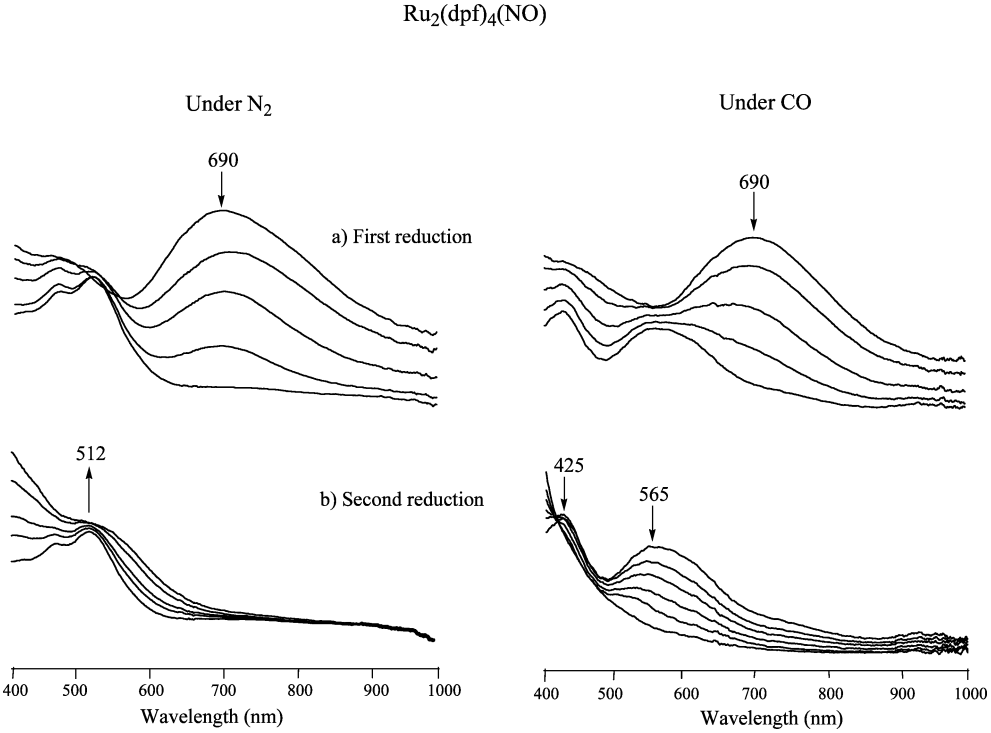

Figure 7. Thin-layer UV−vis spectral changes upon (a) first and (b) second reduction of $Ru_2(dpf)_4(NO)$ in PhCN, 0.2 M TBAP under N_2 or CO.

The formation of $[Ru_2(dpf)_4(NO)(CO)]^-$ and the interaction between NO and CO across the Ru−Ru bond are demonstrated by the infrared spectra of $[Ru_2(dpf)_4(NO)]^-$ in CH_2Cl_2 under N_2 and CO (Figure 6). The ν_{NO} of $[Ru_2(dpf)_4(NO)]^-$ is located at 1712 cm^{-1} under N_2 and 1674 cm^{-1} under CO, and these values are identical to ν_{NO} for $Ru_2(dpf)_4(NO)$ under N_2 and CO after a one-electron reduction (Table 5).

The peak at 1929 cm^{-1} in Figure 6c is due to $Ru_2(dpf)_4(CO)$ generated after the loss of NO. This result agrees with the electrochemical data (Figure 5) as well as with the FTIR spectrum of pure $Ru_2(dpf)_4(CO)$ in the same solution where a peak at the same frequency of 1929 cm^{-1} is obtained (Figure 4 and Table 5).[7]

A summary of the overall electron transfer processes and chemical reactions of the investigated complexes is shown in Scheme 1.

UV−Vis. Table 5 lists the UV−vis spectral data of the investigated complexes along with other related diruthenium complexes. The in-situ UV−vis spectral changes of $Ru_2(dpf)_4(NO)$ and $Ru_2(dpf)_4(NO)_2$ in CH_2Cl_2 or PhCN, 0.2 M TBAP under N_2 and CO, upon reductions and oxidations are shown in Figures 7 and 8.

$Ru_2(dpf)_4(NO)$ exhibits a strong absorption peak at 690 nm under both N_2 and CO. This peak completely disappears upon addition of one electron to the complex, and two new peaks at 464 and 510 nm (under N_2) or 425 and 565 nm (under CO) are observed (Figure 7a and Table 5). A broad band at 512 nm is observed after the second electron is added under N_2 while no bands at all are observed under CO (Figure 7b).

The UV−vis spectrum of $Ru_2(dpf)_4(NO)_2$ in CH_2Cl_2, 0.2 M TBAP, shows only a shoulder at 345 nm, but two broad

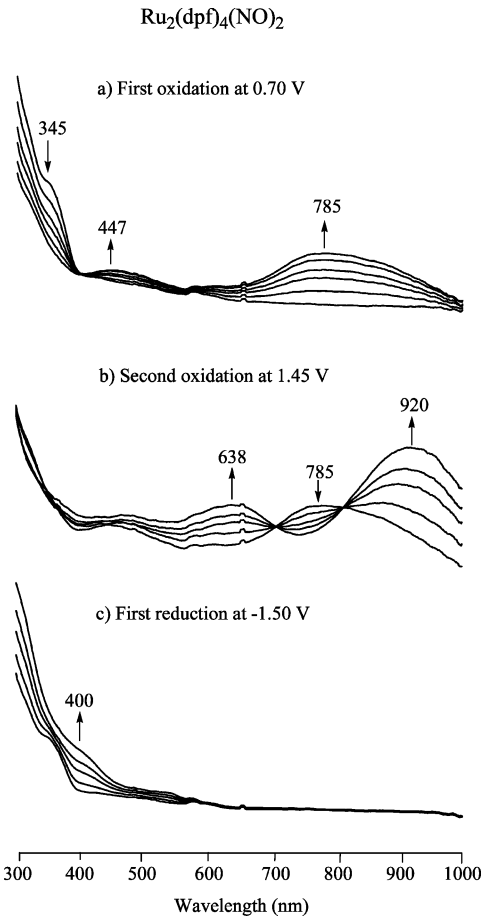

Figure 8. Thin-layer UV−vis spectral changes upon (a) first oxidation, (b) second oxidation, and (c) first reduction of $Ru_2(dpf)_4(NO)_2$ in CH_2Cl_2, 0.2 M TBAP under N_2 or CO.

bands at 447 and 785 nm are observed upon the first oxidation (Figure 8a). Upon the removal of a second electron

from $Ru_2(dpf)_4(NO)_2$, the band at 785 nm disappears, and two new peaks at 638 and 920 nm are seen (Figure 8b). Finally, only a shoulder at 400 nm is seen upon addition of one electron to $Ru_2(dpf)_4(NO)_2$ (Figure 8c). Similar UV−vis spectral changes are obtained under a CO atmosphere, implying the absence of CO coordination to the reduced and oxidized species.

Summary

In this paper, three diruthenium complexes were synthesized with NO and/or CO axial ligands and characterized as to their electrochemical and spectroscopic properties. Two of the complexes, $Ru_2(dpf)_4(NO)$ and $Ru_2(dpf)_4(NO)_2$, were also structurally characterized. One free coordination site on the Ru_2 unit is required in order to have CO binding to the Ru_2 core. The generation of a CO labile complex, $[Ru_2(dpf)_4(NO)(CO)]^-$, reveals the presence of a strong interaction between NO and CO across the metal−metal bond. Finally, electrochemical and infrared spectroscopic studies of $[Ru_2(dpf)_4(NO)]^-$ under CO further confirm the existence of an NO/CO adduct as well as show the presence of communication between NO and CO across Ru−Ru bond.

Acknowledgment. The support of the College of Letters and Sciences and the Graduate School at the University of Wisconsin—Whitewater and the Robert A. Welch Foundation (J.L.B., Grant E-918; K.M.K., Grant E-680) is gratefully acknowledged. We also thank Dr. Zhongjia Tang, Dr. Simon Bott, and Dr. Xiqu Wang for performing the X-ray analyses. We thank Dr. Eric Van Caemelbecke for helpful discussions.

Supporting Information Available: X-ray crystallographic files in CIF format for structural determination of $Ru_2(dpf)_4(NO)$ and $Ru_2(dpf)_4(NO)_2$. This material is available free of charge via the Internet at http://pubs.acs.org.

IC048983E